Environmental Science Nano

ROYAL SOCIETY OF CHEMISTRY

PAPER

View Article Online
View Journal | View Issue

Check for updates

Cite this: *Environ. Sci.: Nano*, 2026, **13**, 1962

Digestive biotransformation of graphene oxide and reduced graphene oxide in the amphibian *Xenopus laevis*: structural, chemical, and toxicological changes

Florian Chapeau, *[a] Eric Pinelli,[a] Chloé Huertas,[b] Lauris Evariste,[b] Gladys Mirey,[b] Emmanuel Flahaut,[c] Armel Descamps-Mandine,[d] Olivier Marsan,[c] Laury Gauthier[a] and Florence Mouchet[a]

Received 9th January 2026,
Accepted 18th March 2026

DOI: 10.1039/d6en00032k

rsc.li/es-nano

Graphene oxide (GO) and reduced graphene oxide (rGO) are carbon-based nanomaterials increasingly used in industrial applications, yet their environmental fate remains poorly understood. Once released into aquatic ecosystems, their interactions with biological systems can alter their physicochemical properties, with implications for their bioavailability and potential toxicity. This study investigates the digestive biotransformation of GO and rGO following ingestion by *Xenopus laevis* larvae, an established aquatic model organism. After 24 hours of exposure, feces containing the digested nanomaterials (dGO and drGO) were collected and analysed using transmission electron microscopy (TEM), Raman spectroscopy, and infrared spectroscopy (FTIR) to assess morphological, structural, and chemical changes. TEM imaging revealed particle alterations, edge erosion, and agglomeration in the digested samples. Raman analysis showed shifts in D* and D″ band positions and decreased defect-related intensity ratios, consistent with partial reduction of GO and rGO. IR spectroscopy confirmed a substantial loss of oxygenated functional groups, with a marked decrease in the oxygen-to-carbon signal ratio in dGO. Notably, carbonyl groups were more strongly reduced than C–O functional groups (epoxy, hydroxyl, alkoxy), suggesting preferential degradation at the sheet edges. rGO, being less oxidized initially, appeared less affected. In parallel, their toxic potential was assessed by measuring cellular viability of bacteria (*Escherichia coli*) and mammalian cell lines (IEC-6 and TR146) exposed to the materials. The results demonstrated that digested GO exhibited lower toxicity towards IEC-6 cells, while retaining antibacterial activity at low concentrations. However, antibacterial effects are lost at higher doses, likely due to agglomeration and reduced bioavailability, whereas rGO and drGO exhibited minimal toxicity across all conditions. These findings highlight the transformative role of digestive processes on graphene-based nanomaterials and underscore the need to consider such biotransformations in environmental risk assessments.

Environmental significance

Risk assessment of graphene-based nanomaterials is still largely based on their as-produced properties, despite their inevitable interaction with biological systems after environmental release. A critical unknown is whether biological processing can alter their structure, reactivity, and toxicity in ways relevant to ecosystems. This study shows that digestive and microbial environments can act as transformation hotspots for graphene materials, modifying their surface chemistry, morphology, and biological effects. By demonstrating that graphene-based nanomaterials are not environmentally static but biologically transformed, this work challenges current assumptions used in environmental nanoscience. It highlights the need to integrate biologically mediated transformation pathways into predictive models of nanomaterial fate, bioavailability, and ecological impact in aquatic systems.

1. Introduction

Carbon-based nanomaterials, particularly graphene oxide (GO) and reduced graphene oxide (rGO), have attracted increasing interest due to their unique properties and multiple applications, notably in electronics, biomedicine,

[a] *Univ Toulouse, CNRS, IRD, Toulouse INP, CRBE, Toulouse, France. E-mail: florian.chapeau@utoulouse.fr*
[b] *Univ Toulouse, EI Purpan, ENVT, INRAE, Toxalim, Toulouse, France*
[c] *Univ Toulouse, CNRS, Toulouse INP, CIRIMAT, Toulouse, France*
[d] *Univ Toulouse, CNRS, INSA, Toulouse INP, Centre de Microcaractérisation Raimond Castaing, Toulouse, France*

and ecosystem bioremediation.[1–4] However, their growing production and use have inevitably led to their release into the environment, particularly in aquatic ecosystems, which serve as final reservoirs for many pollutants. The impact of these nanomaterials on living organisms remains poorly understood, and their persistence and potential toxicity in these environments raise significant concerns. In particular, their ability to interact with biological systems, undergo chemical transformations, and experience changes in ecotoxicological effects remains an open question of major importance for risk assessment.[5,6]

Upon entering ecosystems and interacting with biological matrix, nanomaterials may undergo various physicochemical transformations due to environmental conditions and metabolic processes of organisms.[5,7–10] Transformations can be linked to enzymatic activities,[11–14] or to interactions with microorganisms.[15–17] Several studies have demonstrated that digestive biotransformation of nanomaterials can alter their initial properties, influencing their bioavailability, toxicity, and environmental fate.[18,19] For instance, certain intestinal bacteria have been shown to reduce metal oxide nanoparticles, thereby modifying their reactivity and toxicity.[20] In the case of GO, oxidizing or reducing conditions such as those present in specific microbial and algal environments or induced by enzymatic activity have been reported to modify its functionalization, altering its chemical properties and interactions with biological systems.[15,21,22] However, the fate of GO and rGO after ingestion by aquatic organisms and their potential transformation within the digestive tract remain largely unexplored. A better understanding of these processes, and more broadly, the environmental fate of these nanomaterials, is essential for assessing associated ecotoxicological risks and their potential impact on aquatic ecosystems.[9]

In this context, the aim of this study was to explore the digestive biotransformation of GO and rGO by *Xenopus laevis* larvae, a well-established amphibian model. Following ingestion of nanomaterials by larvae, their faeces were collected to analyze the structural and chemical modifications undergone by digested GO (dGO) and digested rGO (drGO). The primary objective was to identify these transformations and evaluate their impact on the toxicity of the digested materials. Nanomaterial analysis was conducted using electron microscopy, Raman and infrared spectroscopy, enabling the observation of morphological and structural changes as well as chemical alterations related to the functionalization level of GO and rGO. Images and spectral signature analysis allowed the monitoring of structural defects and variations in oxygen-containing functional groups (C═O, C–OH, C–O–C), which are often involved in the toxicity of these materials.[20,23] This *in vivo* approach provided novel insights into the biotransformation of GO into rGO under digestive conditions and highlighted the potential involvement of intestinal microbiota in these processes. Finally, the toxicological consequences of these transformations were evaluated by assessing the viability of *Escherichia coli* bacteria and performing complementary assays on mammalian cell lines. This approach allows us to compare the toxicity of digested and raw materials across multiple biological models with different levels of complexity.

This work proposes an innovative *in vivo* strategy, using a non-axenic aquatic vertebrate model, to study the evolution of graphene-based materials within a biologically complex digestive environment. By combining multi-parameter morphological, structural, chemical, and toxicological analyses, we aim to provide the first integrated characterization of graphene-based biotransformation in an aquatic organism. This approach fills a major gap in our knowledge by demonstrating that biological matrices, particularly through digestive processes and the activity of the associated microbiota, can modulate the environmental behaviour of GO and rGO, a dimension still largely neglected in environmental risk assessment frameworks for nanomaterials.

2. Material and method

2.1. Synthesis and characterization of graphene oxide and reduced graphene oxide

The graphene oxide (GO) used in this study was supplied by Antolin Group and synthesized by oxidizing Grupo Antolin carbon nanofibers (GANF®) using the Hummer's method.[24] The tested reduced graphene oxide (rGO) was produced through a partial reduction of this GO in a hydrogen atmosphere, with a hydrogen flow rate of 5 L h^{-1} at 200 °C for 2 h. The reduction process was carefully controlled to adjust the oxidation level while minimizing any effects on the material's morphology, lateral size, and number of layers. This reduction resulted in rGO samples with similar physical and chemical properties to the original GO, except for changes in surface chemistry and wetting characteristics. The physico-chemical properties of the tested materials are presented in Table 1. Detailed information regarding materials synthesis, physicochemical properties, and initial characterization can be found in previously published works which provide comprehensive synthesis protocols and baseline characterization data.[25]

2.2. *Xenopus* rearing, breeding and exposure conditions

Xenopus rearing and breeding were described in previous works.[26] In summary, spawning in sexually mature *Xenopus* was triggered by an injection of pregnant mare's gonadotropin. Fertilized eggs were raised in tap water filtered through activated charcoal, maintained at 22 ± 2 °C, and fed with ground aquarium fish food (TetraPhyll®, Tetra, Melle, Germany) until they reached stage 50.[27] The *Xenopus* larvae were exposed in groups of 10 to GO at 10 mg L^{-1} and rGO at 10 mg L^{-1}. Control conditions consisting of raw materials without *Xenopus* were also added to serve as a reference without the digestion process (GO and rGO). The exposure was performed in 1 L crystallizing dishes containing reconstituted water (294 mg L^{-1} $CaCl_2{\cdot}2H_2O$; 123.25 mg L^{-1}

Table 1 Physico-chemical characteristics of graphene oxide (GO); reduced graphene oxide (rGO). TEM: transmission electron microscope; HRTEM: high resolution TEM; BET: Brunauer–Emett–Teller; at%: atomic %; GANF®: Grupo Antolin carbon nanofibers

	GO	rGO
Synthesis/production	GANF® processed by Hummers' method	Thermal treatment in hydrogen (5 L h^{-1}) at 200 °C (2 h)
Catalyst	Ni, Fe, Co, Mn	None
Carbon content	69 ± 0.4 at%	83.1 ± 0.5 at%
Oxygen content	30 ± 0.4 at%	16.8 ± 0.3 at%
Number of layers (HRTEM)	1–5	1–5
Lateral size (TEM)	0.2 to 8 μm	0.2 to 8 μm
Specific surface area (BET)	152 ± 0.5 m^2 g^{-1}	156 ± 0.5 m^2 g^{-1}
I_D/I_G (RAMAN)	1.09 ± 0.06	1.26 ± 0.03

$MgSO_4 \cdot 7H_2O$; 64.75 mg L^{-1} $NaHCO_3$; 5.75 mg L^{-1} KCl) for a duration of 24 hours, with no water renewal or feeding during this period. This exposure duration appears sufficient for the *Xenopus* to filter the whole water column. A previous study demonstrated the ability of *Xenopus* larvae to filter all suspended particles in only 4 hours.[28]

2.3. Collection of digested materials

Following 24 hours of exposure, the animals were removed and euthanized. The contents of the crystallizing dishes were filtered through a cellulose nitrate membrane with a 0.22 μm pore size to collect both suspended nanoparticles and those trapped in the faeces. After filtration, the membranes were placed in Eppendorf tubes containing 1.5 mL of Milli-Q water and sonicated for 3 minutes in an ultrasonic bath to resuspend the particles. The control condition underwent the same process to collect faeces, which would later be used to study the matrix effect. After removing the filter, the suspensions were stored in the dark at 4 °C to prevent any material alterations.

2.4. Post-digestion characterization

2.4.1. Transmission electron microscopy (TEM). TEM imaging was performed with a JEOL 2100F TEM operated at 200 kV. The grids were observed with a Gatan Rio16IS Camera in TEM and diffraction modes. Samples were prepared by immersing formvar-coated copper grids into aqueous suspensions of raw and digested graphene. Prior to deposition, each suspension was sonicated using a bath to promote dispersion and ensure homogeneity of the nanomaterials. The grids were gently blotted on filter paper after immersion and allowed to air dry at room temperature before analysis.

2.4.2. RAMAN spectroscopy. The Raman analysis was performed with a Raman Labram HR 800 confocal Microscope (Horiba Scientific). The sample was exposed to the red continue laser at 633 nm with powerful 4.5 mW under an optical microscope Olympus BX21 equipped of objective ×100 (A.N: 09) with a lateral resolution of 0.856 μm and an axial resolution of 3.129 μm. The use of an opacity filter (10% of incident beam) was necessary to preserve the integrity of the samples (limiting sample heating). Each spectrum was acquired with a grating of 600 lines per mm (spectral resolution: 1.8 cm^{-1}) with 25 second of acquisition time and 5 accumulations. All sample were analysed under macro spot (50 × 50 μm) with a piezoelectric mirror system to ensure their homogeneity. Each spectrum was treated by an intensity correction signal (ICS). Prior to data analysis, pre-processing was performed using LabSpec5® software. For each spectrum, baseline correction was applied, and noise reduction was conducted. Deconvolution was performed by fitting the experimental data in the region of interest (1000–1800 cm^{-1}) using Lorentzian, Gaussian, and Gaussian/Lorentzian mixed functions, which are commonly employed for carbonaceous materials. Among these, Gaussian/Lorentzian mixed functions provided the best fit and allowed the identification and retention of four sub-bands: D*, D, D′ D″, and G. For visual representation, spectra were normalized relative to the G band, a standard practice for this type of data analysis.

2.4.3. Fourier-transform infrared spectroscopy (FTIR). IR analysis was performed with a spectrometer IS 50 Thermoscientific® in the spectral range from 4000 to 400 cm^{-1} in reflectance mode (ATR diamond head). Each sample was placed in a drop of ethanol to ensure the evaporation of residual water and limit its impact during analysis. Each analysis was acquired with 64 scans and a spectral resolution of 4 cm^{-1}. The spectra underwent baseline correction with software LabSpec5®, baseline correction was similarly carried out using a linear function, followed by blank (evaporated water + ethanol) subtraction for each sample. Decomposition of the spectra was applied to the region of interest (900–2000 cm^{-1}) following the same approach as for the RAMAN data. Gaussian functions yielded the best fit, enabling the identification of specific functional groups within a massif and the determination of the area under each individual band. Spectra normalization was performed using the "sum" method provided by the software for visual representation. To perform a semi-quantitative assessment of oxygen content, the relative areas of oxygen-related bands (ORB, calculated as the total spectral area minus C═C + O–H (V_2 H_2O) contributions), carbonyl groups (C═O), and C–O related groups (C–OH, C–O–C) were determined by dividing each respective band area by the total integrated area of the spectrum. These ratios were used as indicators of the

degree of surface functionalization of the graphene-based materials.

2.5. Assessment of post digestion toxicity

2.5.1. Antimicrobial properties. The toxicity of nanomaterials after passage through the digestive tract of *Xenopus* was assessed based on their bacteriostatic activity. To this end, *Escherichia coli* bacteria were exposed to various concentrations of raw and digested nanomaterials to evaluate potential variations in toxicity levels. For the bacterial assay, *E. coli* cultures were grown overnight in liquid LB medium. The bacterial suspension was then diluted to an optical density of OD_{600} = 0.1, and different concentrations of nanomaterials chosen from the literature (0, 50, 100 or 500 μg mL^{-1}) were added.[29] The mixture was incubated and stirred continuously (140 rpm) at 37 °C for 4 hours to homogenise the suspension. Following a 1 : 100 000 dilution, 55 μL of the bacterial suspension was spread onto LB agar plates and incubated at 37 °C for 24 hours in a constant-temperature incubator. Bacterial viability was quantified by counting colony-forming units (CFU) (n = 6). For the digested material, the nanomaterials were separated from the fecal residues through successive cycles of brief sonication in an ultrasonic bath followed by centrifugation. Sonication was applied for short periods to detach organic matter from the graphene flakes while minimizing the risk of mechanical alteration to the sheets. Subsequent centrifugation enabled the denser graphene particles to sediment, while lighter organic components remained suspended. The supernatant containing the organic residues was carefully removed and replaced with sterile Milli-Q water. This purification procedure was repeated three times to progressively reduce the presence of residual organic matter. The absence of visible organic debris in the supernatant was verified by optical microscopy prior to further processing. Although this procedure substantially reduced organic contamination, the presence of trace biological material associated with the graphene flakes cannot be completely excluded. The recovered material was then dried, weighed, and resuspended into sterile Milli-Q water to prepare stock suspensions. The raw materials were subjected to the same treatments to avoid methodological bias between samples.

2.5.2. Toxicity towards mammalian epithelial cells. Human TR146 buccal epithelial cells (Sigma–Aldrich) and rat IEC-6 (ATCC CRL-1592) intestinal epithelial cells were cultured respectively in Ham's F12 nutrient mix (Life Technologies, Illkirch, France) and Dulbecco's modified Eagle medium (DMEM, Gibco, Life Technologies) supplemented with 10% fetal calf serum (FBS; Gibco, Life Technologies), 1% penicillin/streptomycin and gentamicin at 50 μg mL^{-1}. Cells were incubated at 37 °C in a humidified 5% CO_2 atmosphere and treated for 24 hours with different concentrations of the tested products (1, 10 and 100 μg mL^{-1}), selected based on a previous work.[30] The complete medium without nanomaterials was used as the negative control group. Three independent experiments were carried out.

Cell viability was evaluated through measurement of cellular ATP using the luminescent CellTiter-Glo® assay (Promega, Madison, USA) according to the manufacturer's instructions. The luminescence was measured using the Spark microplate reader (TECAN, Männedorf, Switzerland) and cell viability is expressed as percentage of the negative control. 45 minutes of treatment with 0.5% of Triton X-100 was used as a positive control (PC), inducing maximal toxic response.

2.6. Statistical analysis

Statistical analysis was performed with Prism 10 software (GraphPad Software Inc., San Diego, CA, USA). Differential effects for antimicrobial properties and cell viability were analyzed by one-way analysis of variance (ANOVA) or Kruskal–Wallis (KW) when the assumption of normal distribution of the data are not met. Tukey or Dunn's *post hoc* tests for multiple comparisons were used following ANOVA or KW respectively when $p < 0.05$. In cellular toxicity, the positive control was tested independently from the test materials to the negative control using Student's T-test. When a significant response is detected, Student's T-test is applied to determine the influence of the digestion process on the toxic response at the same exposure dose. A p-value <0.05 was considered significant ($*p < 0.05$; $**p < 0.01$; $***p < 0.001$; $****p < 0.0001$).

3. Results and discussion

3.1. Post digestion characterization

3.1.1. Transmission electron microscopy. Morphology and structure of materials were studied in the first instance by TEM, the images are presented in Fig. 1A. TEM analysis revealed obvious morphological differences between the raw and digested graphene materials, both in sheet structure and edge definition (Fig. 1A–H). Raw GO and rGO (Fig. 1A and B) appeared as thin, well-dispersed with smooth surfaces and defined edges. Selected area electron diffraction (SAED) patterns confirmed the expected structural order for both materials, with GO and rGO exhibiting characteristic hexagonal symmetry. In contrast, the digested materials, dGO (Fig. 1C) and drGO (Fig. 1D), exhibited marked agglomeration and morphological degradation, enhanced by the adhesion of organic matter on the surface. The sheet-like morphology was significantly disrupted, with the appearance of dense, wrinkled agglomerates and the loss of extended planar domains, suggesting that digestion induced fragmentation or folding. Images focused on the sheet edges confirmed these observations. The edges of raw GO (Fig. 1E) and rGO (Fig. 1F) appeared sharp and well-defined, with smooth linear contours. In contrast, the edges of dGO (Fig. 1G) and drGO (Fig. 1H) exhibited significant irregularity, with irregular wavy borders, indicating edge reorganization or surface erosion. This loss of structural regularity after

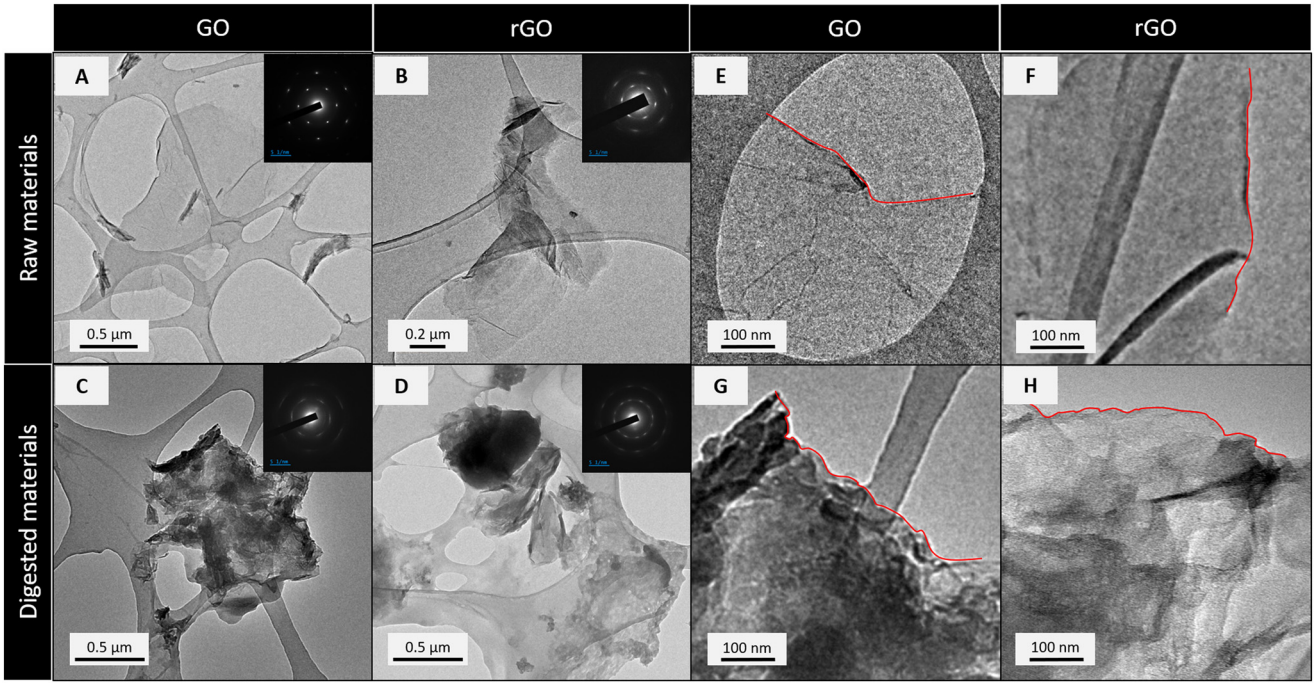

Fig. 1 TEM imaging of raw and digested GO and rGO. TEM images and SAED of raw materials, GO (A) and rGO (B), and digested materials, dGO (C) and drGO (D). Focus on the border of the raw materials, GO (E) and rGO (F), and on the digested materials, dGO (G) and drGO (H). The border of the graphene materials has been underlined by a red line.

digestion suggests that the digestive process can alter both the integrity and morphology of graphene-based materials. Similar observations have been reported in studies investigating microbial or enzymatic interaction with graphene derivatives, where biodegradation or partial reduction was accompanied by the collapse of the two-dimensional structure and increased surface wrinkling.[12,31,32] The observed adhesion of organic matter to the surface of digested materials may reflect interactions with digestive proteins, enzymes, or microbiota-derived biomolecules, which could contribute to the modification of material's properties, as previously demonstrated for GO incubated in

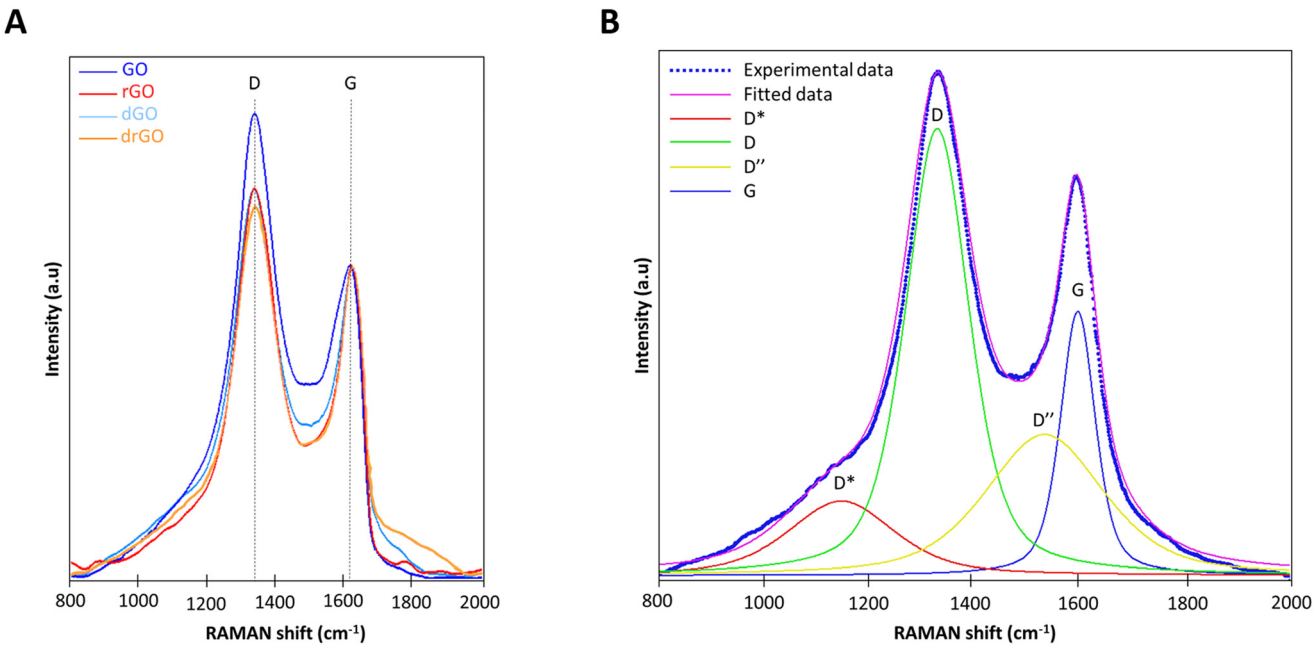

Fig. 2 Raman spectra (normalisation to the G band) for all the samples analysed (A). An example of decomposition of RAMAN spectra (dGO) applied to the data of this study with the four bands obtained (D*, D, D″ and G) (B).

biological fluids or microbial cultures.[33] Moreover, the observed loss of edge definition appears to indicate edge-specific degradation mechanisms, particularly in oxygen-functionalized regions such as epoxides and hydroxylic functions,[34,35] which are known to be sensitive to microbial enzymes and other redox-active organic compounds and could serve as electron acceptors in biological reduction pathways.[36,37] This therefore suggests chemical modifications in addition to physical impairments (agglomeration, edge degradation, crumpling) of these materials. Taken together, these TEM observations provide visual evidence of the physical transformation of GO and rGO during passage through the digestive system of *Xenopus laevis* larvae and hint at potential chemical modifications, supporting the hypothesis of a biotransformation process.

3.1.2. RAMAN analysis. Following the morphological observations of the materials, Raman spectra were measured to assess potential structural and chemical modifications induced by the digestive process (Fig. 2A). First, the spectra obtained for GO, rGO and their digested counterparts exhibited the same number of bands. Two major bands were consistently observed at ~1330 cm^{-1} and ~1595 cm^{-1}, corresponding to the D and G bands, respectively, which are well-established signatures of carbon-based nanomaterials. The D band is generally attributed to structural defects in the crystalline carbon lattice, whereas the G band is associated with the vibration of sp^2-hybridized carbon atoms in graphitic structures.[38,39] To refine the spectral analysis, a decomposition was performed in the 800–2000 cm^{-1} spectral window, revealing two additional bands, D* (~1140–1180 cm^{-1}) and D″ (~1530–1560 cm^{-1}) (Fig. 2B) (SI 1). Several studies have reported that these bands are particularly sensitive to the oxygen content of carbon-based nanomaterials.[40,41] A shift of the D* band toward higher wavenumbers and the D″ band toward lower wavenumbers are generally correlated with a decrease in surface oxygen-containing functional groups.[40,41] The analysis of D* and D″ band positions under different experimental conditions (Fig. 3A) indicated that raw GO exhibited the highest oxygen content, whereas raw rGO and the digested materials exhibited a significant reduction. This behaviour was further confirmed by the position of the D* band, which also suggested a more pronounced decrease in oxygen functionalities in digested GO compared to digested rGO. The assessment of defect density and crystallinity was further explored by analysing the intensity ratios of key bands (Fig. 3B). The I_D/I_G ratio, commonly used to estimate defect density in carbon nanomaterials,[41,42] was higher for raw GO than for the digested materials, which exhibited slightly lower values to those of raw rGO. This result suggests a decrease in structural defects during the digestive process, potentially due to the removal of unstable oxygenated functional groups.[15] A similar trend was observed for the $I_{D''}/I_G$ ratio, which is correlated with material crystallinity,[40] and initially interpreted as evidence of structural reorganization and enhanced graphitization following digestion, a phenomenon previously reported in biological reduction processes.[8,15] However, given that all GO and rGO dispersions were prepared in reconstituted water containing salts and conflicting microscopy observations, an alternative explanation for the observed decrease in I_D/I_G and $I_{D''}/I_G$ ratios must be considered. In aqueous solutions with ionic content, charge screening effects induced by cations and anions can alter the electronic structure of the material, influencing the resonance conditions under which Raman signals intensities are detected.[43,44] The I_D/I_G values for crude GO (1.09) and crude rGO (1.26) in a salt-free medium (Milli-Q water) are higher than those observed in the exposure medium (reconstituted water), suggesting that some of the I_D/I_G decrease initially attributed to biotransformation actually results from salt-induced changes in the state of the nanomaterials, rather than a direct reduction of defects. However, the decrease in the ratios between the D and G bands after digestion suggests an involvement of the digestive process in the reduction of ion-related interference. Digestion therefore seems to have an impact on the surface bonds between ions and graphene. The literature does not seem to indicate significant impacts of salts on the position of the Raman bands unlike the

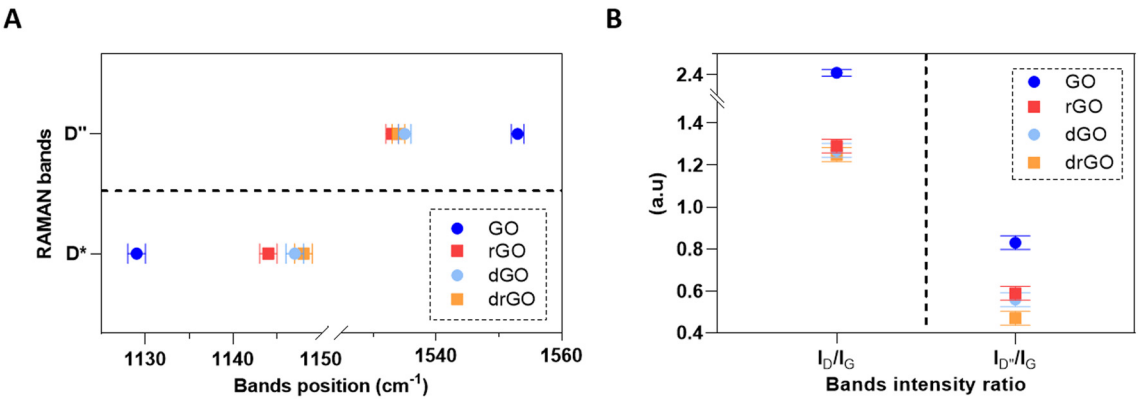

Fig. 3 Positions of RAMAN bands D″ and D* for all samples analysed (A). RAMAN band intensity ratio I_D/I_G and $I_{D''}/I_G$ for all samples analysed (B).

intensities.[43] The interpretation of the positions of the D* and D″ bands is therefore maintained. Other studies have highlighted the ability of organisms such as aquatic algae to reduce GO. However, the authors did not observe graphitization; instead, they reported an increase in the number of structural defects.[21] Therefore, our results suggest that the digestive tract of *Xenopus laevis* larvae may induce partial reduction of GO (and to a lesser extent to rGO), accompanied by a disruption of surface bonds. This phenomenon could result from digestive activity; however, the involvement of the gut microbiota also seems likely. Indeed, sterile *in vitro* studies on human digestive processes have shown no[45] or similar effects on the density of crystal lattice defects and the functionalization of GO and rGO.[46,47] Results from a previous study based on an *in vitro* assay simulating the human ingestion of nanomaterials reported mainly physicochemical changes, such as agglomeration and surface doping, resulting from interactions with digestive fluids. There was no evidence of structural degradation or increased defect density. In contrast, our *in vivo* observations revealed more pronounced transformations following digestive passage in *Xenopus laevis*, including morphological alterations and a reduction of oxygen-containing functional groups in GO. These differences likely reflect the additional biological complexity of living digestive systems, where enzymatic activity and interactions with gut microbiota may contribute to redox processes and surface modifications that cannot be fully reproduced in simplified *in vitro* digestion models. The observed *in vivo* modifications, such as reduction, are often attributed to the grafting of nitrogenous functional groups with an indirect impact on oxygenated functions.[31,48] However, various studies have highlighted the ability of bacteria to reduce carbon nanomaterials through mechanisms involving flavoproteins or cytochromes, among other enzymatic pathways.[8,17,49] The associated microbiota must therefore also be taken into consideration.

However, while Raman spectroscopy is a powerful tool for assessing the structural state of nanomaterials, it does not provide precise information on their chemical functionalization. Results can be potentially mitigated by biological and complex environments. To validate these observations and identify the chemical modifications associated with the observed reduction, complementary analyses were performed using infrared spectroscopy (IR).

3.1.3. Infrared analysis. The infrared spectra recorded in the 4000–800 cm^{-1} range are presented in Fig. 4A. The region of interest for this study lies between 2000–800 cm^{-1}, as higher wavenumbers primarily correspond to O–H and C–H stretching vibrations, which are less relevant for the analysis of GO and rGO are highly subject to experimental conditions. The spectra reveal the presence of key functional groups, with bands located at 1045 cm^{-1}, corresponding to the stretching mode of C–O related groups (C–O–C and C–OH); at 1450 cm^{-1}, attributed to the bending vibration of hydroxyl groups (C–OH); at 1580 cm^{-1} and 1650 cm^{-1}, associated with C–C and C═C + O–H stretching vibrations from water, respectively; and at 1750 cm^{-1}, corresponding to the stretching of carbonyl groups (C═O) located at the sheet edges of GO.[50,51] To better resolve overlapping bands, the spectra were decomposed as illustrated in Fig. 4B. The decomposed band distributions are presented in Fig. 5A, showing the variations in C═O, C═C + O–H, and C–C bonds, and in Fig. 5B, highlighting changes in C–O functional groups. All bands identified in the raw materials were also observed in the digested samples; however, the relative intensity of the bands varied. Although a quantitative analysis cannot be directly inferred, the trends in functional group evolution can be interpreted semi-quantitatively. As expected, raw GO exhibited a higher content of oxygenated groups than raw rGO, while appearing to display a lower number of C═C bonds (conclusion not possible for C═C due to V_2 H_2O). After digestion, the profile of dGO became similar to that of raw rGO, suggesting a loss

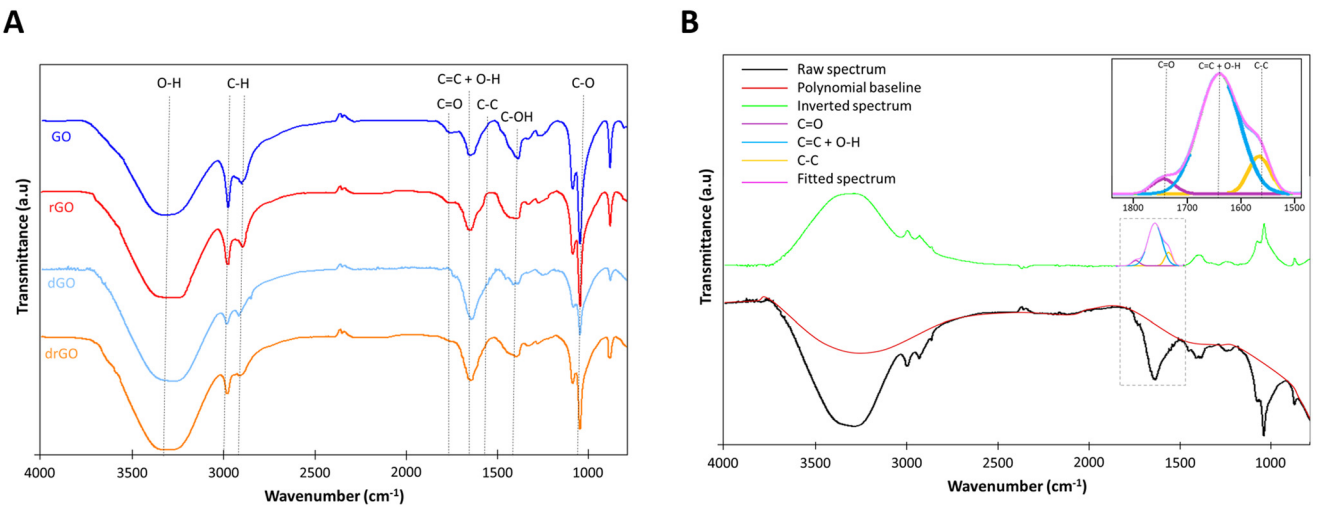

Fig. 4 Normalized infrared spectra for all the samples analysed (A). For the sake of clarity, spectra have been vertically displaced. An example of processing and deconvolution of IR spectra (rGO) applied to the data of this study to identify all the functions of interest (B).

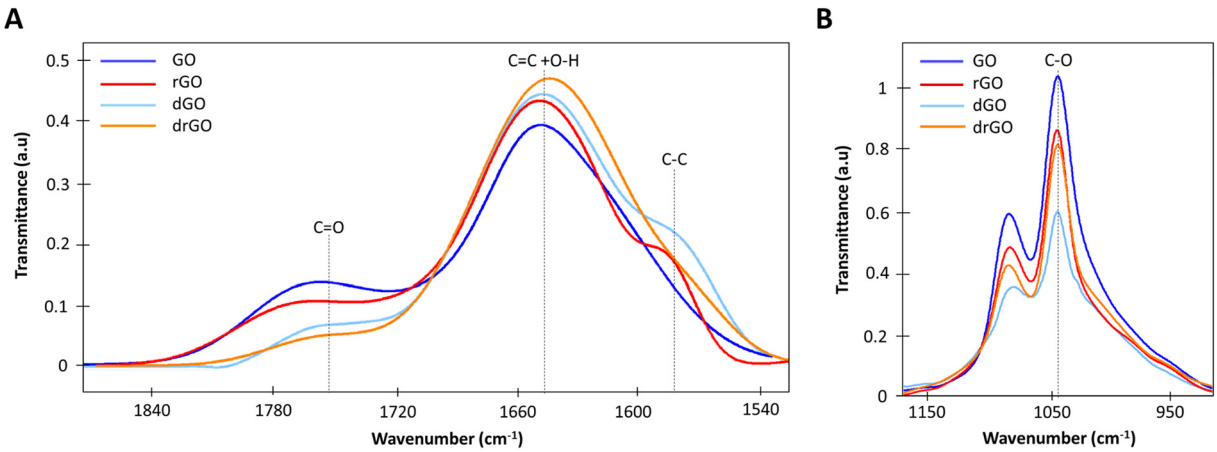

Fig. 5 Deconvoluted infrared spectra for all samples analysed for the specific region 1500 to 1900 cm^{-1} (A) and for the specific region 900 to 1200 cm^{-1} (B).

of oxygen-containing groups and a partial restoration of sp^2 carbon domains. In contrast, drGO appeared to be only marginally affected by the digestive process. This was confirmed by the analysis of IR band area ratios (Table 2). The ratio of oxygen-related bands (ORBs) to the total IR area decreased by 37.5% between raw GO and dGO, indicating a substantial reduction in oxygenated functions. This reduction was not observed for drGO (0.67 *vs.* 0.68 for rGO), whose values remained nearly unchanged. Specifically, the ratios of carbonyl (C═O) and C–O groups followed the same trend, with a marked decrease observed for dGO, suggesting that these groups are particularly labile under digestive conditions. Although C–O groups remain more abundant in absolute terms, the relative decrease in carbonyl (C═O) content was more pronounced for digested GO, with a 50% reduction compared to approximately 34% for C–O related functions. For drGO, only the C═O groups experienced a moderate reduction of approximately 33%. This relative stability of rGO likely reflects its initially lower oxidation state and reduced availability of reactive oxygenated groups,[52] limiting the extent of further transformation during digestion. The modest changes observed for drGO suggest that pre-reduced graphene materials may be less susceptible to digestive alteration as previously observed after stimulated digestion by Bazina and collaborators,[48] which could have implications for their environmental persistence and biological interactions. Although carbonyl groups are typically located at the edges of graphene oxide sheets, which might suggest higher exposure, existing literature indicates that they are generally more stable and less prone to reduction than C–O functional groups, due to electron delocalization and structural context.[53–55] Therefore, the decrease in carbonyl content observed in this study may not result from intrinsic lability, but rather from specific biological or enzymatic targeting mechanisms. In addition, the observed agglomeration of the sheets can modify the accessibility to oxygenated functions and therefore their fate. This spatial constraint may have further favoured the degradation of edge-localized functionalities, despite their inherent stability. The digestive environment of *Xenopus* larvae, possibly mediated by enzymatic or microbial activity, appears to favour the chemical reduction of GO and rGO. Such transformations may have critical implications for the environmental fate and toxicity of these materials by altering their reactivity, bioavailability, and interactions with biological systems.[56,57]

Table 2 Ratio of the integrated area of oxygen-related bands (ORB), carbonyl groups (C═O), and C–O groups (C–O–C & C–OH) to the total area of all bands within the spectral region of interest (800–2000 cm^{-1}) for each condition

	ORB/total ratio	C═O/total ratio	C–O/total ratio
GO	0.8	0.06	0.5
dGO	0.5	0.03	0.33
rGO	0.68	0.03	0.44
drGO	0.67	0.02	0.44

3.2. Post digestion toxicity

Following the identification of digestion-induced physicochemical modifications of GO and rGO, their potential toxicity was assessed using a bacterial growth inhibition assay on *Escherichia coli* at varying concentrations (0, 50, 100, and 500 μg mL^{-1}). The results of Fig. 6A shown that raw GO induced a significant reduction in bacterial growth starting at 50 μg mL^{-1} (Anova, p = 0.0001), with a transient attenuation at 100 μg mL^{-1} (Anova, p = 0.66), followed by a marked inhibitory effect at 500 μg mL^{-1} (Anova, p = <0.0001). In comparison, raw rGO exhibited overall lower toxicity, with a statistically significant effect only at the highest concentration tested of 500 μg mL^{-1} (Anova, p = <0.0001). These thresholds are consistent with values reported in the literature, where antibacterial effects are attributed to both oxidative stress and membrane disruption.[29,58,59] Digested GO (dGO) retained a growth-inhibitory effect at 50 μg mL^{-1} (Anova, p = 0.017), but this

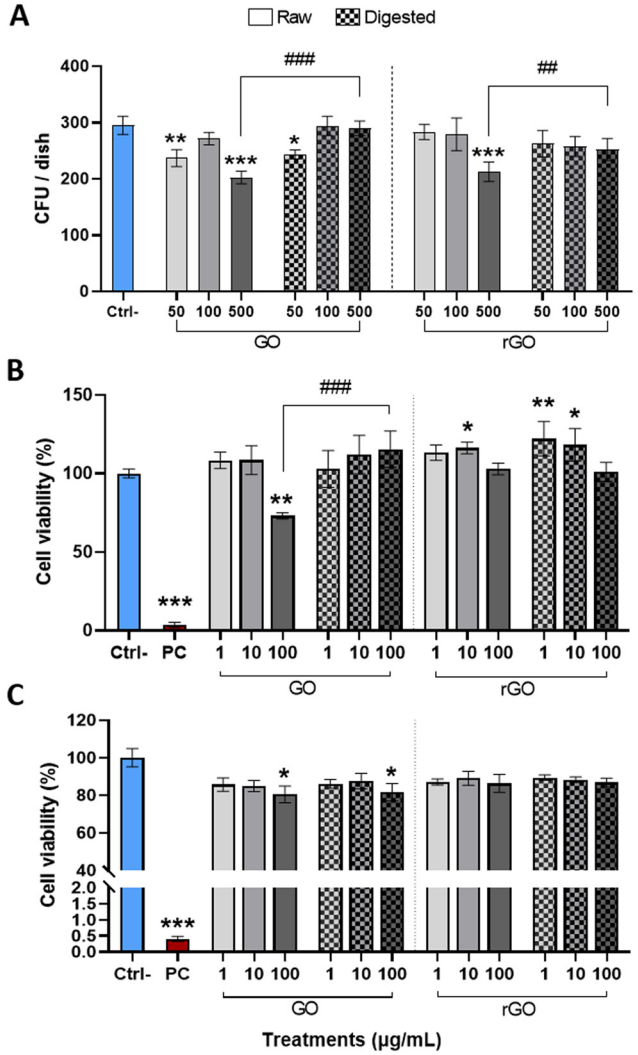

Fig. 6 Assessment of the toxicity of nanomaterials (GO, dGO, rGO and drGO) on A) *E. coli* B) IEC-6 cells and C) TR146 cells. For *E. coli*, the results present the number of colony-forming units (CFU) per dish depending on the concentrations (0, 50, 100 and 500 µg mL^{-1}) after 4 hours of exposure. For cell lines, the viability is expressed as percentage of the negative control group. Data are presented as mean ± SD (n = 6 per condition for *E. coli* and n = 3 for cell lines) (ANOVA followed by Tukey. *: $p < 0.05$; **: $p < 0.01$ and ***: $p < 0.001$). Hashtags (#) indicate levels of significant differences between raw and digested materials.

effect disappeared at 500 µg mL^{-1} (Anova, p = 0.996), suggesting a reduction in toxicity at higher concentrations. Digested rGO (drGO), by contrast, showed no inhibitory effects at any concentration tested, indicating a biological inertness after digestion. However, the persistence of toxicity for dGO at 50 µg mL^{-1} suggests that digestion does not completely neutralize the biological impact of GO. This may reflect the limitations of using high concentration ranges, which can obscure chemical-specific effects such as those related to oxygen functional groups. The disappearance of inhibition at higher doses may instead be attributed to physicochemical transformations altering the behaviour of GO in solution such as increased agglomeration, reduced colloidal stability, or sedimentation under exposure conditions. Thus, beyond their transformation during digestion, the environmental fate of the resulting fecal-associated nanomaterials may be modified, due to the alteration of the mobility and bioavailability of graphene-based materials once released into aquatic environments through biological excretion. In particular, agglomeration and partial reduction may reduce their bioavailability while favoring sedimentation and accumulation in benthic compartments,[60] which can potentially modify their long-term ecological impact. At elevated concentrations, GO flakes are more prone to self-association, and digestion-induced edge defects as well as the presence of surface-bound organic matter may exacerbate these processes. Such changes can reduce effective interactions with bacterial membranes, diminishing observable toxicity. These findings emphasize the importance of considering biologically transformed nanomaterials, rather than pristine materials alone, when assessing the environmental fate and risks of graphene-based contaminants.

In addition to the evaluation of the antimicrobial properties of the materials, we assessed their toxicity towards mammalian cell lines derived from buccal epithelium (TR146) and intestinal cells (IEC-6) exposed during 24 hours to concentrations up to 100 µg mL^{-1} (Fig. 6B and C). Only the highest concentration of GO induced significant viability loss in both cell lines (TR146, KW, p = 0.016 & IEC-6, Anova, $p < 0.001$), but to a lower extend in TR146 compared to IEC-6 cells. Indeed, viability decreased respectively by 19.6 ± 4.4 and 27.1 ± 2%. Interestingly, the digestion process mitigated the GO toxicity at 100 µg mL^{-1} towards IEC-6 cells, while no change in the material toxicity was measured in TR146. Raw rGO did not induce viability loss in TR146 cells (KW, $p > 0.05$), reflecting a lower toxicity compared to raw GO. Differential sensitivity to graphene-based nanomaterials of mammalian cells, including epithelial models, is well documented and strongly depends on cell type and the physicochemical properties of the materials, such as particle size and the oxidation state that are key determinants of toxic responses.[61–63] In IEC-6 cells as well as in cancer cells, previous studies indicated that graphene oxide exposure to a similar dose range led to decreased viability through excessive ROS production, loss of mitochondrial membrane potential and activation of caspase-mediated apoptosis.[30,64] Interestingly, in IEC-6 cells, while rGO did not induced detrimental effects, cellular ATP levels, measured as a proxi for viability, significantly increased (~18%) after exposure to low doses of both raw and digested materials. Some previous studies indicate that GBMs can promote the proliferation of different cancer cell lines when applied at low and non-toxic doses. This effect has been linked to activation of integrin signaling, which subsequently triggers the activation of the downstream PI3K/AKT/mTOR pathway and modulates cell cycle checkpoint proteins, promoting the process of cell mitosis.[65,66] In addition, rGO incorporated at a low dose

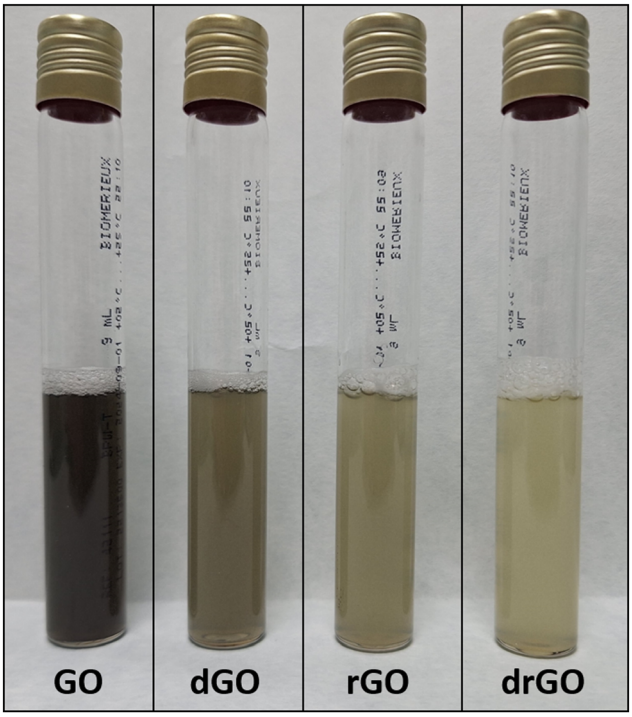

Fig. 7 Photograph of suspensions of the different materials studied at 100 μg mL^{-1} in the bacterial culture medium, at the start of the growth test on *E. coli*. This image highlights the differences in optical properties between GO and rGO, perceptible by the variation in colour of the suspensions as well as an impact of digestion on these properties.

(0.002% w/w) into hydrogels increased the proliferation of endothelial cells, fibroblasts and keratinocytes, as evidenced using MTT assay which allows to assess cell viability based on metabolic activities.[67] Thus, while it remains to be determined, the increased cellular ATP levels detected might result from either an increased cell proliferation or the induction of mitochondrial metabolism.

Although these experiments do not allow to establish a direct correlation between the degree of oxygenation and toxic properties towards bacteria and mammalian cells, it clearly demonstrates that digestion by *Xenopus laevis* larvae modifies properties such as morphology, dispersibility, and agglomeration that can significantly influence biological responses to graphene-based nanomaterials. Additionally, visual observations made at the start of the bacterial assay revealed clear differences in the optical appearance of the dispersions (Fig. 7). While raw GO suspensions appeared characteristically brown and opaque, dGO suspensions at comparable concentrations exhibited a more greyish hue and lower opacity closely resembling the visual aspect of both rGO and drGO. This change in optical properties supports the spectroscopic findings indicating partial reduction of GO during digestion. The shift from brown to grey in GO-based materials is widely associated with the removal of oxygen-containing groups and the partial restoration of the conjugated sp^2 carbon network, which alters light absorption and scattering behaviour.[68,69] In particular, the reappearance of extended π–π conjugation reduces electronic transitions in the visible range, thereby decreasing overall absorbance and giving rise to a lighter, more translucent appearance.[70] These observations provide additional, qualitative support for the chemical transformation of GO under digestive conditions, with implications not only for toxicity but also for the environmental mobility and detection of these nanomaterials in complex media.

The changes observed in GO and rGO after passage through the digestive tract are not only structural and chemical, but also have functional implications, as demonstrated by the toxicity assays. To better understand the origin of these changes and the mechanisms involved, it is essential to examine the digestive environment in which these transformations occur. The digestive system of *Xenopus laevis* larvae remains incompletely characterized and is often described in contradictory terms due to its dynamic evolution throughout the larval stage. Morphologically, it resembles that of herbivorous organisms, featuring an elongated intestinal tract but lacking a clearly defined and functionally mature stomach. While some studies describe the stomach as a semi-differentiated, non-functional structure, others attribute to a more active role in digestion.[71,72] Similarly, physiological characterizations vary. Several reports indicate a near-neutral to slightly alkaline pH throughout the tract, typically between 6.8 and 8.2, based on the activity profiles of enzymes such as glucosidases and alkaline phosphatases.[71,73] In contrast, other studies document a markedly acidic pH in the stomach region, ranging from 1.1 to 4.1, with a return to neutrality in the intestine.[72,74] The digestive contents include typical components such as bile salts, pancreatin, mucus, and the above-mentioned enzymes. Some authors have also questioned whether the chemical environment observed in the gut is solely attributable to the host or is significantly influenced by the associated microbial flora.[74]

These host-related factors may contribute to the superficial modification of GO and rGO. For example, they may alter the surface charge through the adsorption of divalent cations, such as Ca^{2+} and Mg^{2+}. They may also induce protonation or hydrolytic cleavage in acidic microenvironments. Alternatively, they may act through digestive enzymes, which are capable of mediating limited electron-transfer reactions.[14,75,76] However, these processes alone are unlikely to fully explain the significant reduction in oxygenated functional groups, especially in light of data from *in vitro* enzymatic assays and sterile digestion models replicating the human gastrointestinal tract. In enzymatic systems, oxidation, rather than reduction, is most frequently observed as the dominant pathway. Similarly, in digestion models, and in the absence of established and complex microbial populations, GO and rGO undergo no[47] or moderate structural modifications, generally related to surface adsorption or slight functionalization, under relatively reactive conditions (*e.g.*, acidic and highly variable

pH, presence of strong enzymes such as peroxidases) compared to our biological model.[31,46,48]

This suggests that the gut microbiota may play a central role in mediating the transformations observed. Numerous studies have shown that specific bacterial taxa can reduce GO through various mechanisms.[77–79] Model species such as *Shewanella oneidensis*, *Geobacter sulfurreducens*, and certain strains of *Bacillus* and *Pseudomonas* have demonstrated the ability to donate electrons directly to GO, resulting in deoxygenation and partial restoration of the sp^2 carbon lattice.[77,79–81] Additional microbial reduction pathways include the generation of reactive oxygen species (ROS), the use of GO as a terminal electron acceptor in anaerobic respiration,[79] and enzymatic reduction by reductases, hydrogenases or peroxidases *via* electron generation.[12,13,36,76] In this study, the identification of bacterial families (SI 2 and 3) within the gut microbiota of *Xenopus* larvae such as *Desulfovibrionaceae*, *Rikenellaceae*, *Lachnospiraceae* and *Fusobacteriaceae* provides further support, as many of these taxa are known to engage in extracellular electron transfer or sulfo-reductive metabolism and redox activity.[82–84] Specifically, *Rikenella microfusus*, found to be the most abundant identified species in our dataset (~18.8 ± 6.4%), has been experimentally demonstrated to possess extracellular electron transfer capabilities.[85] Moreover, the high microbial diversity observed (~265 OTUs) suggests the presence of additional, possibly uncharacterized, bacterial contributors to the reduction process. Under the semi-anaerobic or microaerophilic conditions that prevail in the larval digestive tract, these microorganisms could facilitate the partial reduction and degradation of oxygen-rich functional groups, in a consistent manner with mechanisms described in "green" reduction processes.[78] Finally, at the molecular level, all the hypothetical reduction pathways presented rely on the same fundamental mechanism: the transfer of electrons to the oxidized functional groups of the graphene network. By providing reducing equivalents to the carbonyl, epoxy, or hydroxyl groups, microbial, enzymatic, or redox processes can cleave the C–O bonds and partially restore sp^2 conjugation, thus inducing the deoxygenation of the graphene oxide.[36,86]

In summary, the observed loss of toxicity, morphological degradation, and depletion of oxygenated functional groups following digestion in *Xenopus* larvae gut, most likely result from a synergistic interaction between the physicochemical conditions of the gut and microbiota-mediated reduction. These findings underscore the importance of considering microbial contributions when evaluating the environmental transformation and long-term impact of graphene-based nanomaterials.

4. Conclusion

Given the rise of graphene-based nanomaterials, it is essential to understand their environmental behaviour and potential transformations in biological systems. This study aimed to investigate how ingestion by aquatic vertebrates, particularly *Xenopus* larvae, can alter the structure, chemistry, and toxicity of graphene oxide (GO) and its reduced forms (rGO). This work represents, to our knowledge, the first *in vivo* demonstration of the digestive reduction and, more broadly, of the biotransformation of GBMs by an aquatic vertebrate, providing an unprecedented view of how these materials evolve once released into realistic environmental conditions.[9] In this digestive context, numerous observations revealed notable biotransformation of both materials. Transmission electron microscopy revealed marked morphological degradation after digestion, particularly at the leaflet edges, as well as an accumulation of surface-bound organic matter. These structural alterations suggest the involvement of enzymatic or microbiota-mediated processes. Raman spectroscopy revealed a reduction in structural defects and shifts in oxygen-sensitive bands, consistent with partial reduction. These observations were corroborated by infrared (IR) spectroscopy, which indicated a significant loss of oxygen-containing functional groups, particularly carbonyls, in digested GO. The preferential degradation of edge-localized carbonyl functionalities likely reflects their increased sensitivity to biological reduction. Functionally, these chemical and morphological transformations were associated with changes in antibacterial activity and cytotoxicity towards mammalian cells. While toxic for cell lines at high doses, GO retained some antimicrobial activities only at low concentrations but lost this effect at higher doses. For rGO, even if it remained largely inert for bacteria before and after digestion, both forms were able to promote cellular proliferation or metabolism. The decrease in microbial toxicity at high concentrations appears to be correlated with increased agglomeration and sedimentation, suggesting that colloidal behaviour and dispersibility play a critical role in biological interactions, in addition to surface chemistry, likely by decreasing bioaccessibility. Overall, these findings show that GO and rGO behave as dynamic, evolving contaminants whose environmental fate can be strongly reshaped by digestive and microbiota-driven processes. These results underscore the need to incorporate biologically mediated transformation pathways, particularly those involving gut microbiota processes, into environmental risk assessment frameworks for graphene-based materials. Characterization of as-synthesized carbon nanomaterials is not sufficient for the assessment of their environmental impact and must also be performed in biological environments. More broadly, this study supports the relevance of *in vivo* ecotoxicological models and opens promising avenues to explore the ecological persistence and biotransformation potential of engineered nanomaterials in realistic environmental settings. It also highlights the need to better describe in the literature the level of reduction of "rGO", which can vary substantially among studies and has profound implications for interpreting environmental behaviour and toxicity.

Ethical standards

The experimental procedures were performed under the authorization of the vertebrate animal experimentation facility n°B31113002 and were approved by the Ethics Committee n°073 (authorization n°#34208-2021120214298638 v3), in accordance with French and European legislation on animal experimentation (European Directive 2010/63/EU).

Author contributions

Florian Chapeau: writing – review & editing, writing – original draft, visualization, investigation, formal analysis, data curation, conceptualization. Eric Pinelli: writing – review & editing, supervision, conceptualization. Chloé Huertas: investigation, formal analysis. Lauris Evariste: supervision, conceptualization, formal analysis. Gladys Mirey: supervision, conceptualization. Emmanuel Flahaut: writing – review & editing, resources, methodology, data curation. Armel Descamps-Mandine: writing – review & editing, investigation, resources, methodology. Olivier Marsan: writing – review & editing, investigation, resources, methodology. Laury Gauthier: writing – review & editing, funding acquisition. Florence Mouchet: writing – review & editing, supervision, project administration, funding acquisition, conceptualization.

Conflicts of interest

The authors declare that they have no known competing financial interests or personal relationships that could have appeared to influence the work reported in this paper.

Data availability

The data that support the findings of this study are available from the corresponding authors upon request. The supplementary information (SI) includes, RAMAN deconvoluted spectra and the detailed protocol for *Xenopus laevis* intestinal microbiota analysis, along with the associated datasets used in the discussion part.

Supplementary information is available. See DOI: https://doi.org/10.1039/d6en00032k.

Acknowledgements

This project has received funding from the European Union's Horizon 2020 research and innovation programme under grant agreement No. 881603. This research was also supported by the French Ministry of National Education, Higher Education and Research. This study has been partially supported through the grant EUR TESS N°ANR-18-EURE-0018 in the framework of the Programme des Investissements d'Avenir. The authors acknowledge the Centre de Microcaractérisation Raymond Castaing (UMS 3623, CNRS/University of Toulouse III – Paul Sabatier) for providing access to analytical facilities and technical support. We would like to thanks Julien Vignard and Christel Cartier from Toxalim for the technical support with cell toxicity assessment.

References

1 B. Bhushan, P. Negi, A. Nayak and S. Goyal, Graphene Composites for Water Remediation: An Overview of Their Advanced Performance with Focus on Challenges and Future Prospects, *Adv. Compos. Hybrid Mater.*, 2024, **8**(1), 55, DOI: 10.1007/s42114-024-01088-x.

2 D. Maiti, X. Tong, X. Mou and K. Yang, Carbon-Based Nanomaterials for Biomedical Applications: A Recent Study, *Front. Pharmacol.*, 2019, **9**, DOI: 10.3389/fphar.2018.01401.

3 S. Nasir, M. Z. Hussein, Z. Zainal and N. A. Yusof, Carbon-Based Nanomaterials/Allotropes: A Glimpse of Their Synthesis, Properties and Some Applications, *Materials*, 2018, **11**(2), 295, DOI: 10.3390/ma11020295.

4 L. S. Sundar and M. W. Ashraf, Synthesis and Characterization Methods of Graphene Oxide Nanomaterial for Biomedical and Toxicity Applications: A Comprehensive Review, *Inorg. Chem. Commun.*, 2025, **174**, 113936, DOI: 10.1016/j.inoche.2025.113936.

5 Y. Zhao, Y. Liu, X. Zhang and W. Liao, Environmental Transformation of Graphene Oxide in the Aquatic Environment, *Chemosphere*, 2021, **262**, 127885, DOI: 10.1016/j.chemosphere.2020.127885.

6 B. Suarez-Merino, V. Adam, S. Gressler, F. Part, N. Bossa, M. Pelin, M. Carlin, C. F. Candotto, G. Caorsi, H. Hong, B. Nowack, D. Beloin-Saint-Pierre, E. Briñas, S. García-Carpintero, M. Durán-Prado, E. Vázquez, M. Prato, P. Wick and J. H. Baker, Regulatory Challenges and Risk Assessment of Graphene-Enabled Products: Insights for Safe Commercialisation in Europe, *2D Mater.*, 2025, **12**(4), DOI: 10.1088/2053-1583/ade4a5.

7 W.-C. Hou, I. Chowdhury, D. G. Goodwin Jr., W. M. Henderson, D. H. Fairbrother, D. Bouchard and R. G. Zepp, Photochemical Transformation of Graphene Oxide in Sunlight, *Environ. Sci. Technol.*, 2015, **49**(6), 3435–3443, DOI: 10.1021/es5047155.

8 E. C. Salas, Z. Sun, A. Lüttge and J. M. Tour, Reduction of Graphene Oxide via Bacterial Respiration, *ACS Nano*, 2010, **4**(8), 4852–4856, DOI: 10.1021/nn101081t.

9 S. Vranic, R. Kurapati, K. Kostarelos and A. Bianco, Biological and Environmental Degradation of Two-Dimensional Materials, *Nat. Rev. Chem.*, 2025, **9**(3), 173–184, DOI: 10.1038/s41570-024-00680-5.

10 J. Zhao, Z. Wang, J. C. White and B. Xing, Graphene in the Aquatic Environment: Adsorption, Dispersion, Toxicity and Transformation, *Environ. Sci. Technol.*, 2014, **48**(17), 9995–10009, DOI: 10.1021/es5022679.

11 M. Chen, X. Qin and G. Zeng, Biodegradation of Carbon Nanotubes, Graphene, and Their Derivatives, *Trends Biotechnol.*, 2017, **35**(9), 836–846, DOI: 10.1016/j.tibtech.2016.12.001.

12 R. Kurapati, C. Martìn, V. Palermo, Y. Nishina and A. Bianco, Biodegradation of Graphene Materials Catalyzed by Human

Eosinophil Peroxidase, *Faraday Discuss.*, 2021, **227**, 189–203, DOI: 10.1039/C9FD00094A.

13 G. Lalwani, W. Xing and B. Sitharaman, Enzymatic Degradation of Oxidized and Reduced Graphene Nanoribbons by Lignin Peroxidase, *J. Mater. Chem. B*, 2014, **2**(37), 6354–6362, DOI: 10.1039/C4TB00976B.

14 A. B. Seabra, A. J. Paula and N. Durán, Redox-Enzymes, Cells and Micro-Organisms Acting on Carbon Nanostructures Transformation: A Mini-Review, *Biotechnol. Prog.*, 2013, **29**(1), 1–10, DOI: 10.1002/btpr.1673.

15 O. Akhavan and E. Ghaderi, Escherichia Coli Bacteria Reduce Graphene Oxide to Bactericidal Graphene in a Self-Limiting Manner, *Carbon*, 2012, **50**(5), 1853–1860, DOI: 10.1016/j.carbon.2011.12.035.

16 J. Du, X. Hu and Q. Zhou, Graphene Oxide Regulates the Bacterial Community and Exhibits Property Changes in Soil, *RSC Adv.*, 2015, **5**(34), 27009–27017, DOI: 10.1039/C5RA01045D.

17 Z. Guo, C. Xie, P. Zhang, J. Zhang, G. Wang, X. He, Y. Ma, B. Zhao and Z. Zhang, Toxicity and Transformation of Graphene Oxide and Reduced Graphene Oxide in Bacteria Biofilm, *Sci. Total Environ.*, 2017, **580**, 1300–1308, DOI: 10.1016/j.scitotenv.2016.12.093.

18 M. I. Setyawati, Z. Zhao and K. W. Ng, Transformation of Nanomaterials and Its Implications in Gut Nanotoxicology, *Small*, 2020, **16**(36), 2001246, DOI: 10.1002/smll.202001246.

19 I. S. Sohal, Y. K. Cho, K. S. O'Fallon, P. Gaines, P. Demokritou and D. Bello, Dissolution Behavior and Biodurability of Ingested Engineered Nanomaterials in the Gastrointestinal Environment, *ACS Nano*, 2018, **12**(8), 8115–8128, DOI: 10.1021/acsnano.8b02978.

20 J. Zhang, W. Guo, Q. Li, Z. Wang and S. Liu, The Effects and the Potential Mechanism of Environmental Transformation of Metal Nanoparticles on Their Toxicity in Organisms, *Environ. Sci.: Nano*, 2018, **5**(11), 2482–2499, DOI: 10.1039/C8EN00688A.

21 P. Braylé, E. Pinelli, B. Schoefs, E. Flahaut, J. Silvestre, L. Gauthier and M. Barret, Effects of Graphene Oxide on the Diatom Nitzschia Palea Are Associated with Carbon Cycling Disturbance, *Carbon*, 2024, **226**, 119224, DOI: 10.1016/j.carbon.2024.119224.

22 K. Wu, S. Ouyang, Z. Tao, X. Hu and Q. Zhou, Algal Extracellular Polymeric Substance Compositions Drive the Binding Characteristics, Affinity, and Phytotoxicity of Graphene Oxide in Water, *Water Res.*, 2024, 121908, DOI: 10.1016/j.watres.2024.121908.

23 C. Xie, P. Zhang, Z. Guo, X. Li, Q. Pang, K. Zheng, X. He, Y. Ma, Z. Zhang and I. Lynch, Elucidating the Origin of the Surface Functionalization - Dependent Bacterial Toxicity of Graphene Nanomaterials: Oxidative Damage, Physical Disruption, and Cell Autolysis, *Sci. Total Environ.*, 2020, **747**, 141546, DOI: 10.1016/j.scitotenv.2020.141546.

24 W. S. Hummers, Jr. and R. E. Offeman, Preparation of Graphitic Oxide, *J. Am. Chem. Soc.*, 1958, **80**(6), 1339, DOI: 10.1021/ja01539a017.

25 L. Evariste, L. Lagier, P. Gonzalez, A. Mottier, F. Mouchet, S. Cadarsi, P. Lonchambon, G. Daffe, G. Chimowa, C. Sarrieu, E. Ompraret, A.-M. Galibert, C. Matei Ghimbeu, E. Pinelli, E. Flahaut and L. Gauthier, Thermal Reduction of Graphene Oxide Mitigates Its In Vivo Genotoxicity Toward Xenopus Laevis Tadpoles, *Nanomaterials*, 2019, **9**(4), 584, DOI: 10.3390/nano9040584.

26 F. Mouchet, P. Landois, E. Sarremejean, G. Bernard, P. Puech, E. Pinelli, E. Flahaut and L. Gauthier, Characterisation and in Vivo Ecotoxicity Evaluation of Double-Wall Carbon Nanotubes in Larvae of the Amphibian Xenopus Laevis, *Aquat. Toxicol.*, 2008, **87**(2), 127–137, DOI: 10.1016/j.aquatox.2008.01.011.

27 P. D. Nieuwkoop and J. Faber, Normal Table of Xenopus Laevis (Daudin). A Systematical and Chronological Survey of the Development from the Fertilized Egg Till the End of Metamorphosis, *Q. Rev. Biol.*, 1958, **33**(1), 85, DOI: 10.1086/402265.

28 L. Evariste, F. Mouchet, E. Pinelli, E. Flahaut, L. Gauthier and M. Barret, Gut Microbiota Impairment Following Graphene Oxide Exposure Is Associated to Physiological Alterations in Xenopus Laevis Tadpoles, *Sci. Total Environ.*, 2023, **857**, 159515, DOI: 10.1016/j.scitotenv.2022.159515.

29 S. Qiang, Z. Li, L. Zhang, D. Luo, R. Geng, X. Zeng, J. Liang, P. Li and Q. Fan, Cytotoxic Effect of Graphene Oxide Nanoribbons on Escherichia Coli, *Nanomaterials*, 2021, **11**(5), 1339, DOI: 10.3390/nano11051339.

30 W. Feng, J. Wang, B. Li, Y. Liu, D. Xu, K. Cheng and J. Zhuang, Graphene Oxide Leads to Mitochondrial-Dependent Apoptosis by Activating ROS-P53-mPTP Pathway in Intestinal Cells, *Int. J. Biochem. Cell Biol.*, 2022, **146**, 106206, DOI: 10.1016/j.biocel.2022.106206.

31 D. Bitounis, D. Parviz, X. Cao, C. A. Amadei, C. D. Vecitis, E. M. Sunderland, B. D. Thrall, M. Fang, M. S. Strano and P. Demokritou, Synthesis and Physicochemical Transformations of Size-Sorted Graphene Oxide during Simulated Digestion and Its Toxicological Assessment against an In Vitro Model of the Human Intestinal Epithelium, *Small*, 2020, **16**(21), 1907640, DOI: 10.1002/smll.201907640.

32 G. P. Kotchey, B. L. Allen, H. Vedala, N. Yanamala, A. A. Kapralov, Y. Y. Tyurina, J. Klein-Seetharaman, V. E. Kagan and A. Star, The Enzymatic Oxidation of Graphene Oxide, *ACS Nano*, 2011, **5**(3), 2098–2108, DOI: 10.1021/nn103265h.

33 K. Swetha, S. Samantaray, F. A. L. S. Silva, F. C. Silva, B. Freitas, J. A. C. Incorvia, J. R. Fernandes, A. Jayaraj, S. Banerjee, N. Sadananda Singh, F. D. Magalhães, A. M. Pinto and R. Kurapati, Biodegradability of Partially Reduced Nanographene Oxide by Human, Plant and Microbial Enzymes: Impact of Magnetic Nanoparticles, *Carbon*, 2024, **229**, 119486, DOI: 10.1016/j.carbon.2024.119486.

34 K. Erickson, R. Erni, Z. Lee, N. Alem, W. Gannett and A. Zettl, Determination of the Local Chemical Structure of Graphene Oxide and Reduced Graphene Oxide, *Adv. Mater.*, 2010, **22**(40), 4467–4472, DOI: 10.1002/adma.201000732.

35 S. Mikhailov, *Physics and Applications of Graphene: Experiments*, BoD – Books on Demand, 2011.
36 Y. Lu, L. Zhong, L. Tang, H. Wang, Z. Yang, Q. Xie, H. Feng, M. Jia and C. Fan, Extracellular Electron Transfer Leading to the Biological Mediated Production of Reduced Graphene Oxide, *Chemosphere*, 2020, **256**, 127141, DOI: 10.1016/j.chemosphere.2020.127141.
37 Y. Su, X. Gao and J. Zhao, Reaction Mechanisms of Graphene Oxide Chemical Reduction by Sulfur-Containing Compounds, *Carbon*, 2014, **67**, 146–155, DOI: 10.1016/j.carbon.2013.09.073.
38 A. C. Ferrari and J. Robertson, Interpretation of Raman Spectra of Disordered and Amorphous Carbon, *Phys. Rev. B: Condens. Matter Mater. Phys.*, 2000, **61**(20), 14095–14107, DOI: 10.1103/PhysRevB.61.14095.
39 B. Ma, R. D. Rodriguez, A. Ruban, S. Pavlov and E. Sheremet, The Correlation between Electrical Conductivity and Second-Order Raman Modes of Laser-Reduced Graphene Oxide, *Phys. Chem. Chem. Phys.*, 2019, **21**(19), 10125–10134, DOI: 10.1039/C9CP00093C.
40 S. Claramunt, A. Varea, D. López-Díaz, M. M. Velázquez, A. Cornet and A. Cirera, The Importance of Interbands on the Interpretation of the Raman Spectrum of Graphene Oxide, *J. Phys. Chem. C*, 2015, **119**(18), 10123–10129, DOI: 10.1021/acs.jpcc.5b01590.
41 D. López-Díaz, M. López Holgado, J. L. García-Fierro and M. M. Velázquez, Evolution of the Raman Spectrum with the Chemical Composition of Graphene Oxide, *J. Phys. Chem. C*, 2017, **121**(37), 20489–20497, DOI: 10.1021/acs.jpcc.7b06236.
42 N. Sharma, V. Sharma, Y. Jain, M. Kumari, R. Gupta, S. K. Sharma and K. Sachdev, Synthesis and Characterization of Graphene Oxide (GO) and Reduced Graphene Oxide (rGO) for Gas Sensing Application, *Macromol. Symp.*, 2017, **376**(1), 1700006, DOI: 10.1002/masy.201700006.
43 P. K. Ang, S. Wang, Q. Bao, J. T. L. Thong and K. P. Loh, High-Throughput Synthesis of Graphene by Intercalation –Exfoliation of Graphite Oxide and Study of Ionic Screening in Graphene Transistor, *ACS Nano*, 2009, **3**(11), 3587–3594, DOI: 10.1021/nn901111s.
44 F. Chen, J. Xia and N. Tao, Ionic Screening of Charged-Impurity Scattering in Graphene, *Nano Lett.*, 2009, **9**(4), 1621–1625, DOI: 10.1021/nl803922m.
45 M. Kucki, P. Rupper, C. Sarrieu, M. Melucci, E. Treossi, A. Schwarz, V. León, A. Kraegeloh, E. Flahaut, E. Vázquez, V. Palermo and P. Wick, Interaction of Graphene-Related Materials with Human Intestinal Cells: An in Vitro Approach, *Nanoscale*, 2016, **8**(16), 8749–8760, DOI: 10.1039/C6NR00319B.
46 Ó. Cebadero-Domínguez, L. Diez-Quijada, S. López, S. Sánchez-Ballester, M. Puerto, A. M. Cameán and A. Jos, Impact of Gastrointestinal Digestion In Vitro Procedure on the Characterization and Cytotoxicity of Reduced Graphene Oxide, *Nanomaterials*, 2023, **13**(16), 2285, DOI: 10.3390/nano13162285.
47 D. Guarnieri, P. Sánchez-Moreno, A. E. Del Rio Castillo, F. Bonaccorso, F. Gatto, G. Bardi, C. Martín, E. Vázquez, T. Catelani, S. Sabella and P. P. Pompa, Biotransformation and Biological Interaction of Graphene and Graphene Oxide during Simulated Oral Ingestion, *Small*, 2018, **14**(24), 1800227, DOI: 10.1002/smll.201800227.
48 L. Bazina, D. Bitounis, X. Cao, G. M. DeLoid, D. Parviz, M. S. Strano, H.-Y. G. Lin, D. C. Bell, B. D. Thrall and P. Demokritou, Biotransformations and Cytotoxicity of Graphene and Inorganic Two-Dimensional Nanomaterials Using Simulated Digestions Coupled with a Triculture in Vitro Model of the Human Gastrointestinal Epithelium, *Environ. Sci.: Nano*, 2021, **8**(11), 3233–3249, DOI: 10.1039/D1EN00594D.
49 N. Ma, B. Zhang, J. Liu, P. Zhang, Z. Li and Y. Luan, Green Fabricated Reduced Graphene Oxide: Evaluation of Its Application as Nano-Carrier for pH-Sensitive Drug Delivery, *Int. J. Pharm.*, 2015, **496**(2), 984–992, DOI: 10.1016/j.ijpharm.2015.10.081.
50 E. Fuente, J. A. Menéndez, M. A. Díez, D. Suárez and M. A. Montes-Morán, Infrared Spectroscopy of Carbon Materials: A Quantum Chemical Study of Model Compounds, *J. Phys. Chem. B*, 2003, **107**(26), 6350–6359, DOI: 10.1021/jp027482g.
51 J. Guerrero-Contreras and F. Caballero-Briones, Graphene Oxide Powders with Different Oxidation Degree, Prepared by Synthesis Variations of the Hummers Method, *Mater. Chem. Phys.*, 2015, **153**, 209–220, DOI: 10.1016/j.matchemphys.2015.01.005.
52 E. T. Mombeshora and E. Muchuweni, Dynamics of Reduced Graphene Oxide: Synthesis and Structural Models, *RSC Adv.*, 2023, **13**(26), 17633–17655, DOI: 10.1039/d3ra02098c.
53 S. Lin, J. Tang, K. Zhang, Y. Chen, R. Gao, H. Yin and L.-C. Qin, Tuning Oxygen-Containing Functional Groups of Graphene for Supercapacitors with High Stability, *Nanoscale Adv.*, 2023, **5**(4), 1163–1171, DOI: 10.1039/D2NA00506A.
54 N.-F. Chiu, T.-Y. Huang and H.-C. Lai, Graphene Oxide Based Surface Plasmon Resonance Biosensors, *Adv. Graphene Sci.*, 2013, DOI: 10.5772/56221.
55 A. Rawal, S. H. Che Man, V. Agarwal, Y. Yao, S. C. Thickett and P. B. Zetterlund, Structural Complexity of Graphene Oxide: The Kirigami Model, *ACS Appl. Mater. Interfaces*, 2021, **13**(15), 18255–18263, DOI: 10.1021/acsami.1c01157.
56 B. Fadeel, C. Bussy, S. Merino, E. Vázquez, E. Flahaut, F. Mouchet, L. Evariste, L. Gauthier, A. J. Koivisto, U. Vogel, C. Martín, L. G. Delogu, T. Buerki-Thurnherr, P. Wick, D. Beloin-Saint-Pierre, R. Hischier, M. Pelin, F. Candotto Carniel, M. Tretiach, F. Cesca, F. Benfenati, D. Scaini, L. Ballerini, K. Kostarelos, M. Prato and A. Bianco, Safety Assessment of Graphene-Based Materials: Focus on Human Health and the Environment, *ACS Nano*, 2018, **12**(11), 10582–10620, DOI: 10.1021/acsnano.8b04758.
57 A. Wang, K. Pu, B. Dong, Y. Liu, L. Zhang, Z. Zhang, W. Duan and Y. Zhu, Role of Surface Charge and Oxidative Stress in Cytotoxicity and Genotoxicity of Graphene Oxide towards Human Lung Fibroblast Cells, *J. Appl. Toxicol.*, 2013, **33**(10), 1156–1164, DOI: 10.1002/jat.2877.
58 S. Liu, T. H. Zeng, M. Hofmann, E. Burcombe, J. Wei, R. Jiang, J. Kong and Y. Chen, Antibacterial Activity of Graphite, Graphite Oxide, Graphene Oxide, and Reduced

Graphene Oxide: Membrane and Oxidative Stress, *ACS Nano*, 2011, **5**(9), 6971–6980, DOI: 10.1021/nn202451x.

59 K. Olczak, W. Jakubowski and W. Szymański, Bactericidal Activity of Graphene Oxide Tests for Selected Microorganisms, *Materials*, 2023, **16**(11), 4199, DOI: 10.3390/ma16114199.

60 Y. Han, C. D. Knightes, D. Bouchard, R. Zepp, B. Avant, H.-S. Hsieh, X. Chang, B. Acrey, W. M. Henderson and J. Spear, Simulating Graphene Oxide Nanomaterial Phototransformation and Transport in Surface Water, *Environ. Sci.: Nano*, 2019, **6**(1), 180–194, DOI: 10.1039/C8EN01088A.

61 S. Achawi, J. Pourchez, B. Feneon and V. Forest, Graphene-Based Materials In Vitro Toxicity and Their Structure–Activity Relationships: A Systematic Literature Review, *Chem. Res. Toxicol.*, 2021, **34**(9), 2003–2018, DOI: 10.1021/acs.chemrestox.1c00243.

62 Ó. Cebadero-Domínguez, A. Jos, A. M. Cameán and G. M. Cătunescu, Hazard Characterization of Graphene Nanomaterials in the Frame of Their Food Risk Assessment: A Review, *Food Chem. Toxicol.*, 2022, **164**, 113014, DOI: 10.1016/j.fct.2022.113014.

63 S. Mittal, V. Kumar, N. Dhiman, L. K. S. Chauhan, R. Pasricha and A. K. Pandey, Physico-Chemical Properties Based Differential Toxicity of Graphene Oxide/Reduced Graphene Oxide in Human Lung Cells Mediated through Oxidative Stress, *Sci. Rep.*, 2016, **6**(1), 39548, DOI: 10.1038/srep39548.

64 A. Jarosz, M. Skoda, I. Dudek and D. Szukiewicz, Oxidative Stress and Mitochondrial Activation as the Main Mechanisms Underlying Graphene Toxicity against Human Cancer Cells, *Oxid. Med. Cell. Longevity*, 2016, **2016**(1), 5851035, DOI: 10.1155/2016/5851035.

65 W. Liu, C. Sun, C. Liao, L. Cui, H. Li, G. Qu, W. Yu, N. Song, Y. Cui, Z. Wang, W. Xie, H. Chen and Q. Zhou, Graphene Enhances Cellular Proliferation through Activating the Epidermal Growth Factor Receptor, *J. Agric. Food Chem.*, 2016, **64**(29), 5909–5918, DOI: 10.1021/acs.jafc.5b05923.

66 Z. Zheng, A. Halifu, J. Ma, L. Liu, Q. Fu, B. Yi, E. Du, D. Tian, Y. Xu, Z. Zhang and J. Zhu, Low-Dose Graphene Oxide Promotes Tumor Cells Proliferation by Activating PI3K-AKT-mTOR Signaling via Cellular Membrane Protein Integrin αV, *Environ. Pollut.*, 2023, **330**, 121817, DOI: 10.1016/j.envpol.2023.121817.

67 S. R. ur Rehman, R. Augustine, A. A. Zahid, R. Ahmed, M. Tariq and A. Hasan, Reduced Graphene Oxide Incorporated GelMA Hydrogel Promotes Angiogenesis For Wound Healing Applications, *Int. J. Nanomed.*, 2019, **14**, 9603–9617, DOI: 10.2147/IJN.S218120.

68 K. P. Loh, Q. Bao, G. Eda and M. Chhowalla, Graphene Oxide as a Chemically Tunable Platform for Optical Applications, *Nat. Chem.*, 2010, **2**(12), 1015–1024, DOI: 10.1038/nchem.907.

69 R. Su, S. F. Lin, D. Q. Chen and G. H. Chen, Study on the Absorption Coefficient of Reduced Graphene Oxide Dispersion, *J. Phys. Chem. C*, 2014, **118**(23), 12520–12525, DOI: 10.1021/jp500499d.

70 H. Otsuka, K. Urita, N. Honma, T. Kimuro, Y. Amako, R. Kukobat, T. J. Bandosz, J. Ukai, I. Moriguchi and K. Kaneko, Transient Chemical and Structural Changes in Graphene Oxide during Ripening, *Nat. Commun.*, 2024, **15**(1), 1708, DOI: 10.1038/s41467-024-46083-4.

71 J. Hourdry, A. L'Hermite and R. Ferrand, Changes in the Digestive Tract and Feeding Behavior of Anuran Amphibians during Metamorphosis, *Physiol. Zool.*, 1996, **69**(2), 219–251.

72 M. Ikuzawa, S. Yasumasu, K. Kobayashi, T. Inokuchi and I. Iuchi, Stomach Remodeling-associated Changes of H^+ /K^+ -ATPase β Subunit Expression in Xenopus Laevis and H^+ /K^+ -ATPase-dependent Acid Secretion in Tadpole Stomach, *J. Exp. Zool., Part A*, 2004, **301**(12), 992–1002, DOI: 10.1002/jez.a.127.

73 I. Griffiths, The Form and Function of the Fore-Gut in Anuran Larvae (Amphibia, Salientia) with Particular Reference to the Manicotto Glandulare, *Proc. Zool. Soc. London*, 1961, **137**(2), 249–283, DOI: 10.1111/j.1469-7998.1961.tb05901.x.

74 R. Kujat and B. Droba, Acid Proteolytic Activity in the Fore Gut of the Xenopus Laevis Larvae, *Comp. Biochem. Physiol., Part A: Mol. Integr. Physiol.*, 1979, **63**(4), 543–545, DOI: 10.1016/0300-9629(79)90192-0.

75 S. Park, K.-S. Lee, G. Bozoklu, W. Cai, S. T. Nguyen and R. S. Ruoff, Graphene Oxide Papers Modified by Divalent Ions—Enhancing Mechanical Properties via Chemical Cross-Linking, *ACS Nano*, 2008, **2**(3), 572–578, DOI: 10.1021/nn700349a.

76 Y.-Z. Wang, H.-C. Liu, J.-X. Wang, S. Nawab, S. Z. Abbas, D. Zhu, J.-L. Mi, L. Zou and Y.-C. Yong, Enzymatic Reduction of Graphene Oxide by a Secreted Hydrogenase, *Biochem. Eng. J.*, 2024, **204**, 109220, DOI: 10.1016/j.bej.2024.109220.

77 P. Guo, F. Xiao, Q. Liu, H. Liu, Y. Guo, J. R. Gong, S. Wang and Y. Liu, One-Pot Microbial Method to Synthesize Dual-Doped Graphene and Its Use as High-Performance Electrocatalyst, *Sci. Rep.*, 2013, **3**(1), 3499, DOI: 10.1038/srep03499.

78 M. Kurian, Recent Progress in the Chemical Reduction of Graphene Oxide by Green Reductants–A Mini Review, *Carbon Trends*, 2021, **5**, 100120, DOI: 10.1016/j.cartre.2021.100120.

79 R. Singh, K. Alshaghdali, A. Saeed, M. A. Kausar, F. M. Aldakheel, S. Anwar, D. Mishra and M. Srivastava, Prospects of Microbial-Engineering for the Production of Graphene and Its Derivatives: Application to Design Nanosystms for Cancer Theranostics, *Semin. Cancer Biol.*, 2022, **86**, 885–898, DOI: 10.1016/j.semcancer.2021.05.017.

80 E. C. Salas, Z. Sun, A. Lüttge and J. M. Tour, Reduction of Graphene Oxide via Bacterial Respiration, *ACS Nano*, 2010, **4**(8), 4852–4856, DOI: 10.1021/nn101081t.

81 C. Vargas, R. Simarro, J. A. Reina, L. F. Bautista, M. C. Molina and N. González-Benítez, New Approach for Biological Synthesis of Reduced Graphene Oxide, *Biochem. Eng. J.*, 2019, **151**, 107331, DOI: 10.1016/j.bej.2019.107331.

82 F. Carbonero, A. C. Benefiel, A. H. Alizadeh-Ghamsari and H. R. Gaskins, Microbial Pathways in Colonic Sulfur Metabolism and Links with Health and Disease, *Front. Physiol.*, 2012, **3**, DOI: 10.3389/fphys.2012.00448.

83 V. Gonzalez, J. Abarca-Hurtado, A. Arancibia, F. Claverías, M. R. Guevara and R. Orellana, Novel Insights on Extracellular Electron Transfer Networks in the Desulfovibrionaceae Family: Unveiling the Potential Significance of Horizontal Gene Transfer, *Microorganisms*, 2024, **12**(9), 1796, DOI: 10.3390/microorganisms12091796.

84 M. Vacca, G. Celano, F. M. Calabrese, P. Portincasa, M. Gobbetti and M. De Angelis, The Controversial Role of Human Gut Lachnospiraceae, *Microorganisms*, 2020, **8**(4), 573, DOI: 10.3390/microorganisms8040573.

85 M. Grattieri, K. Hasan, R. D. Milton, S. Abdellaoui, M. Suvira, B. Alkotaini and S. D. Minteer, Investigating Extracellular Electron Transfer of Rikenella Microfusus: A Recurring Bacterium in Mixed-Species Biofilms, *Sustainable Energy Fuels*, 2017, **1**(7), 1568–1572, DOI: 10.1039/C7SE00270J.

86 W. Lai, Z. Wang, Y. Li, X. Wang, Y. Liu and X. Liu, Radical Mechanism for the Reduction of Graphene Derivatives Initiated by Electron-Transfer Reactions, *J. Phys. Chem. C*, 2018, **122**(15), 8473–8479, DOI: 10.1021/acs.jpcc.8b01941.